

Entanglement properties of superconducting qubits coupled to a semi-infinite transmission line

Yang-Qing Guo(郭羊青), Ping-Xing Chen(陈平形), and Jian Li(李剑)

Citation: Chin. Phys. B, 2023, 32 (**6**): 060302. DOI: 10.1088/1674-1056/acc0fa
Journal homepage: http://cpb.iphy.ac.cn; http://iopscience.iop.org/cpb

What follows is a list of articles you may be interested in

Quantum computation and simulation with superconducting qubits

Kaiyong He(何楷泳), Xiao Geng(耿霄), Rutian Huang(黄汝田), Jianshe Liu(刘建设), and Wei Chen(陈炜)
Chin. Phys. B, 2021, 30 (**8**): 080304. DOI: 10.1088/1674-1056/ac16cf

Universal quantum control based on parametric modulation in superconducting circuits

Dan-Yu Li(李丹宇), Ji Chu(储继), Wen Zheng(郑文), Dong Lan(兰栋), Jie Zhao(赵杰), Shao-Xiong Li(李邵雄), Xin-Sheng Tan(谭新生), and Yang Yu(于扬)
Chin. Phys. B, 2021, 30 (**7**): 070308. DOI: 10.1088/1674-1056/ac01c3

Invariants-based shortcuts for fast generating Greenberger—Horne—Zeilinger state among three superconducting qubits

Jing Xu(徐晶), Lin Yu(于琳), Jin-Lei Wu(吴金雷), Xin Ji(计新)
Chin. Phys. B, 2017, 26 (**9**): 090301. DOI: 10.1088/1674-1056/26/9/090301

Fast generating *W* state of three superconducting qubits via Lewis-Riesenfeld invariants

Lin Yu(于琳), Jing Xu(徐晶), Jin-Lei Wu(吴金雷), Xin Ji(计新)
Chin. Phys. B, 2017, 26 (**6**): 060306. DOI: 10.1088/1674-1056/26/6/060306

Creating nitrogen–vacancy ensembles in diamond for coupling with flux qubit

Ya-Rui Zheng(郑亚锐), Jian Xing(邢健), Yan-Chun Chang(常彦春), Zhi-Guang Yan(闫智广), Hui Deng(邓辉), Yu-Lin Wu(吴玉林), Li Lü(吕力), Xin-Yu Pan(潘新宇), Xiao-Bo Zhu(朱晓波), Dong-Ning Zheng(郑东宁)
Chin. Phys. B, 2017, 26 (**2**): 020305. DOI: 10.1088/1674-1056/26/2/020305

Entanglement properties of superconducting qubits coupled to a semi-infinite transmission line

Yang-Qing Guo(郭羊青)[1], Ping-Xing Chen(陈平形)[1], and Jian Li(李剑)[2,3,4,†]

[1] *Department of Physics, National University of Defense Technology, Changsha* 410073, *China*
[2] *Shenzhen Institute for Quantum Science and Engineering, Southern University of Science and Technology, Shenzhen* 518055, *China*
[3] *International Quantum Academy, Shenzhen* 518048, *China*
[4] *Guangdong Provincial Key Laboratory of Quantum Science and Engineering, Southern University of Science and Technology, Shenzhen* 518055, *China*

(Received 18 January 2023; revised manuscript received 2 March 2023; accepted manuscript online 3 March 2023)

Quantum entanglement, a key resource in quantum information processing, is reduced by interaction between the quantum system concerned and its unavoidable noisy environment. Therefore it is of particular importance to study the dynamical properties of entanglement in open quantum systems. In this work, we mainly focus on two qubits coupled to an adjustable environment, namely a semi-infinite transmission line. The two qubits' relaxations, through individual channels or collective channel or both, can be adjusted by the qubits' transition frequencies. We examine entanglement dynamics in this model system with initial Werner state, and show that the phenomena of entanglement sudden death and revival can be observed. Due to the hardness of preparing the Werner state experimentally, we introduce a new type of entangled state called pseudo-Werner state, which preserves as much entangling property as the Werner state, and more importantly, it is experiment friendly. Furthermore, we provide detailed procedures for generating pseudo-Werner state and studying entanglement dynamics with it, which can be straightforwardly implemented in a superconducting waveguide quantum electrodynamics system.

Keywords: superconducting qubits, quantum entanglement, Werner state

PACS: 03.67.Bg, 12.20.–m, 85.25.Am **DOI:** 10.1088/1674-1056/acc0fa

1. Introduction

Quantum entanglement, which expresses the quantum correlation of the subsystems in a larger quantum system, is one of the unique phenomena in quantum physics. Presently, quantum entanglement has been treated as a crucial resource required for almost all aspects of quantum information processing,[1] e.g., quantum key distribution,[2,3] quantum teleportation,[4,5] dense coding,[6,7] remote state preparation,[8,9] and quantum computation.[10] However, the presence of unavoidable interaction between a quantum system and its environment, which results in relaxation and decoherence, becomes the major obstacle for manipulating entangled systems in an open quantum world. In consequence, preparation and dynamics of entangled states have drawn much attention in the last two decades. There has a lot of effort in studying the variation of entanglement due to decoherence in different systems, and some novel phenomena have been found, e.g., entanglement sudden death (ESD) and revival etc.[11–21]

A typical model for studying ESD[11] consists of two non-interacting qubits coupling to independent environmental noises, respectively. By further replacing the two independent environmental noises with a multimode vacuum field and adding the interaction between the qubits, resurrection of the disappeared entanglement can happen.[14] The ESD phenomenon was experimentally verified with atom ensembles[12] and photon pairs[13] in 2007, and revival after ESD was experimentally observed with two photons in 2010.[15] After that, a system of two superconducting qubits driven by coherent microwave fields was theoretically studied, and stationary entangled states were obtained in a certain region of the parameter space.[16] Meanwhile, entanglement transferred from the bipartite system to the reservoirs,[17] the scenario of interacted qubits contacting with different environments (reservoirs) at zero temperature,[18] as well as the influence of correlation between initial environments on entanglement evolution of two-body systems[19] was also considered.

Previous work has already systematically studied entanglement dynamics under different kinds of couplings between the qubits and the reservoirs theoretically, nevertheless, there lacks of setup to verify these dynamics experimentally in a single system. Very recent progress in superconducting waveguide quantum electrodynamics (QED)[22–26] provides such an opportunity to experimentally investigate ESD and revival on chip. In this context, we mainly focus on exploring the entanglement dynamics with various combinations of collective and individual relaxation channels as well as qubit–qubit couplings, which can be controlled by qubits' frequencies, in a waveguide QED system. We consider a class of X shape initial states (only the diagonal and anti-diagonal elements of the

†Corresponding author. E-mail: lij33@sustech.edu.cn

© 2023 Chinese Physical Society and IOP Publishing Ltd

density matrix are non-zero), which are commonly used for studying bipartite entanglement properties.

Our work is structured as follows. In Section 2, we give the model and describe the kinematic equation of the system. In Section 3, we detail the dependence of entanglement time evolution on different values of collective, individual relaxations and coupling of the qubits. In Section 4, we show a procedure for experimentally observing ESD and revival in a superconducting waveguide QED system. The conclusion is in Section 5.

2. Physical model

Here we consider a system of two small two-level atoms (qubits) coupled to a semi-infinite transmission line, very similar to the one studied in Ref. [22], as shown in Fig. 1. The semi-infinite transmission line has a coplanar waveguide (CPW) form, and its left-hand-side end (LHSE) is shorted to the ground. The qubits are small in comparison to the wavelengths of the CPW's bosonic modes at their transition frequencies. Thus, these two qubits (a and b) can be considered as point-like objects. The length of the CPW between the LHSE and qubit-a's coupling position is x_1, and the length between qubit-a's and qubit-b's coupling positions is x_2, as illustrated in Fig. 1. $x_2 = 2x_1$ will be considered through out the following discussions. An auxiliary qubit (c) will be required for preparing entangled states of qubit-a and qubit-b in Section 4. However in this section, let us ignore the existence of qubit-c.

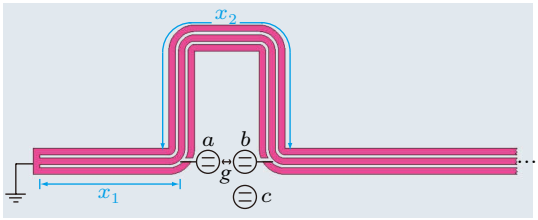


Fig. 1. The schematic model of two qubits (a and b) coupled to a semi-infinite waveguide. There is a switchable coupling g between qubit-a and qubit-b. An auxiliary qubit (c) is tunably coupled to qubit-b, and is only used for preparing initial entangled states.

If there is no direct coupling g between qubit-a and qubit-b, the system we consider here is exactly the same as the small atoms + mirror model discussed in Ref. [22]. We assume that the transition frequencies of qubit-a and qubit-b are similar, $\omega_a \approx \omega_b$, and that the bare coupling strengths between qubit-a,b and the CPW (the rates describe how fast photon can emit from qubit-a,b to the CPW without any interference) are the same, $\gamma_a = \gamma_b \equiv \gamma$. We further consider that the two qubits have similar intrinsic non-radiative relaxation rate $\gamma_{\rm nr}$, which is much smaller than γ. Thus, the master equation of this system can be written as[22]

$$\dot{\rho} = -\mathrm{i}[H,\rho] + \Gamma_a \mathcal{D}[\sigma_-^a]\rho + \Gamma_b \mathcal{D}[\sigma_-^b]\rho + \Gamma_{\rm col}\left[\sigma_-^a\rho\sigma_+^b + \sigma_-^b\rho\sigma_+^a - \frac{1}{2}\left\{\sigma_+^a\sigma_-^b + \sigma_+^b\sigma_-^a, \rho\right\}\right], \quad (1)$$

where $\Gamma_a = \gamma(1+\cos\phi) + \gamma_{\rm nr}$ and $\Gamma_b = \gamma(1+\cos 3\phi) + \gamma_{\rm nr}$ are individual relaxation rates of qubit-a and qubit-b, respectively. $\Gamma_{\rm col} = \gamma(\cos\phi + \cos 2\phi)$ is the collective relaxation rate of the two qubits. The system Hamiltonian

$$H = \left(\omega_a + \frac{\gamma}{2}\sin\phi\right)\frac{\sigma_z^a}{2} + \left(\omega_b + \frac{\gamma}{2}\sin 3\phi\right)\frac{\sigma_z^b}{2} + \frac{\gamma}{2}(\sin\phi + \sin 2\phi)\left(\sigma_-^a\sigma_+^b + \sigma_+^a\sigma_-^b\right), \quad (2)$$

where $\phi = 2\pi x_2/\lambda$ denotes the phase shift between the two coupling positions of the two qubits, and λ is the wavelength determined by qubit-a's transition frequency ω_a. $\sigma_{-(+)}^m$ is the lowering (raising) operator of qubit-m, σ_z^m represents the Pauli z-matrix of qubit-m, and $\mathcal{D}[A]\rho = A\rho A^\dagger - (1/2)\{A^\dagger A, \rho\}$.

From the Hamiltonian Eq. (2), one finds that couplings to the semi-infinite transmission line can induce frequency shifts $\delta\omega_1 = (\gamma/2)\sin\phi$, $\delta\omega_2 = (\gamma/2)\sin 3\phi$ for the qubits, and that a qubit–qubit exchange coupling with strength $g_x = \gamma(\sin\phi + \sin 2\phi)/2$ is also induced. Since in a waveguide QED setup, the length x_2 (also x_1) is fixed when the chip is fabricated, therefore the phase shift ϕ is only dependent on wavelength λ (which is controlled by the qubit transition frequency). Thus in Fig. 2, $\delta\omega_1$, $\delta\omega_2$, and g_x are plotted as functions of λ. In Fig. 3, the individual and collective relaxation rates as functions of λ are also plotted.

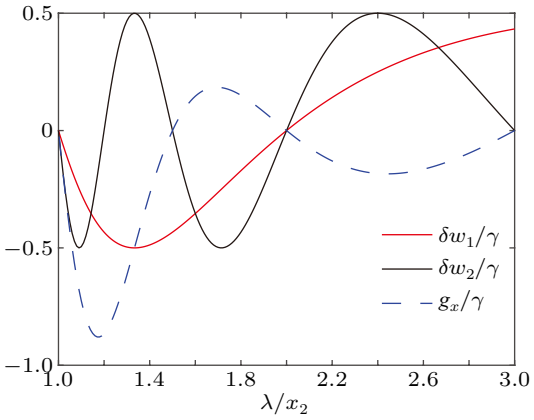


Fig. 2. Qubit frequency shifts $\delta\omega_1$, $\delta\omega_2$ and exchange coupling strength g_x versus wavelength λ.

When preparing an entangled initial state of qubit-a and qubit-b, finite couplings between the two qubits are required, and zero individual relaxation rate of each qubit is also desired for high state fidelity (the collective relaxation rate may not necessarily be zero). From Fig. 3 we can find that, only at $\lambda = 2x_2$ both individual relaxation rates Γ_a and Γ_b are zero (assuming the intrinsic relaxation rate $\gamma_{\rm nr}$ is negligibly small here); but from Fig. 2 we also get zero qubit–qubit exchange coupling g_x at this wavelength. Thus we need an extra switchable qubit–qubit exchange coupling g, as shown in Fig. 1,

to help generate high fidelity entangled state. In a superconducting waveguide QED system, this switchable exchange coupling can be realized by using a third qubit as a tunable coupler.[27]

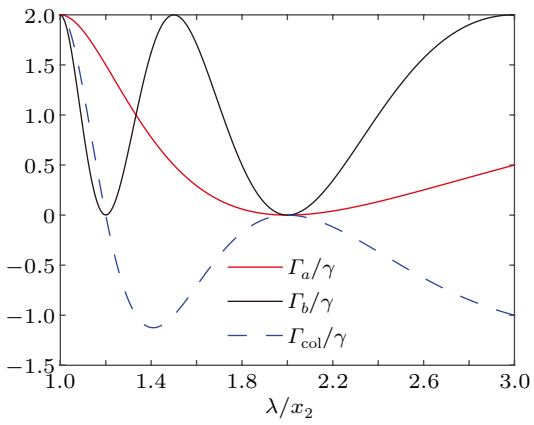


Fig. 3. The individual relaxation rates Γ_a, Γ_b and the collective relaxation rate $\Gamma_{\rm col}$ versus wavelength λ. The intrinsic relaxation rate $\gamma_{\rm nr}=0$ is taken.

3. Dynamics of entanglement

For a bipartite system, Wootters' concurrence C[28] is a convenient entanglement measure, especially for X shape states which retain X form[16] during the evolution governed by the master equation. Now we focus on a subclass of X shape states — the Werner state,[29] which is defined as

$$\begin{aligned}\rho_{\rm W} &= \frac{1-f}{3}\boldsymbol{I}_4+\frac{4f-1}{3}\left|\Psi^-\right\rangle\left\langle\Psi^-\right| \\ &= \frac{1}{3}\begin{pmatrix}1-f & 0 & 0 & 0\\ 0 & (1+2f)/2 & (1-4f)/2 & 0\\ 0 & (1-4f)/2 & (1+2f)/2 & 0\\ 0 & 0 & 0 & 1-f\end{pmatrix}, \end{aligned} \tag{3}$$

where $|\Psi^-\rangle=(|01\rangle-|10\rangle)/\sqrt{2}$ represents the Bell singlet state, f is called fidelity, and $0.25\le f\le 1$. To solve the master equation with initial Werner state, we follow the procedure described in Ref. [30] (see Appendix A).

In the following calculations, we take the intrinsic nonradiative relaxation rate $\gamma_{\rm nr}=2\pi\times 0.03$ MHz (see Ref. [23]), and the bare coupling strength between the qubits and the CPW $\gamma=2\pi\times 5$ MHz.

3.1. No exchange coupling, no collective relaxation

By observing Figs. 2 and 3, one may easily find that the most trivial wavelength is $\lambda/x_2=2$, at which the qubit–qubit exchange coupling $g_x=0$, and the collective relaxation rate $\Gamma_{\rm col}=0$. In this case, after the initial entangled state is prepared, there is no way to induce extra entanglement, therefore only ESD can happen.

Figure 4 shows time evolution of the concurrence for that the qubits are initially in the Werner state, and frequency is tuned to $\lambda=2x_2$. Without qubit–qubit coupling and common reservoir (collective relaxation), concurrence shows sudden death for $f\le 0.714$, which is well known for the Werner state.[11]

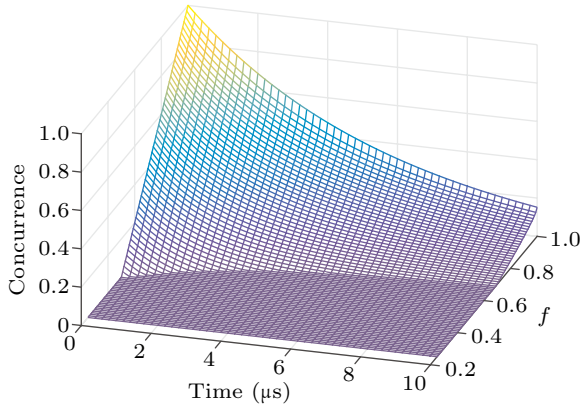


Fig. 4. Time evolution of the concurrence for initial Werner state $\rho_{\rm W}$ at $\lambda/x_2=2$.

3.2. No exchange coupling, finite collective relaxation

When qubit-a's and qubit-b's frequencies are tuned to $\lambda=1.5x_2$, the exchange coupling g_x vanishes, and the collective relaxation rate $\Gamma_{\rm col}=-\gamma=-2\pi\times 5$ MHz.

The time evolution of the concurrence for the Werner initial state is plotted in Fig. 5 for this case. The concurrence experiences sudden death even with $f>0.8$, due to the boosted individual relaxations Γ_a and Γ_b. However, because of the existence of the common reservoir, entanglement revives after sudden death. The reviviscent concurrence decays slowly for the rather large individual relaxation rates $\Gamma_a=2\pi\times 2.53$ MHz and $\Gamma_b=2\pi\times 10.03$ MHz.

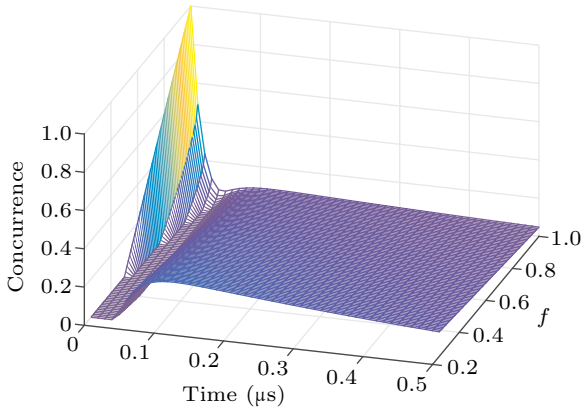


Fig. 5. Time evolution of the concurrence for initial Werner state $\rho_{\rm W}$ at $\lambda/x_2=1.5$.

3.3. Finite exchange coupling, no collective relaxation

By tuning the qubits' frequencies to $\lambda=1.2x_2$, the exchange coupling strength $g_x\approx -0.866\gamma=-2\pi\times 4.33$ MHz, and the collective relaxation rate $\Gamma_{\rm col}=0$.

In this case, after ESD there is an entanglement revival, as shown in Fig. 6. Unlike the case discussed in Subsection 3.2, here the reviviscent concurrence decays to zero quite

fast, even though here the individual relaxation rates $\Gamma_a = 2\pi \times 7.53$ MHz and $\Gamma_b = 2\pi \times 0.03$ MHz are smaller than those in Subsection 3.2.

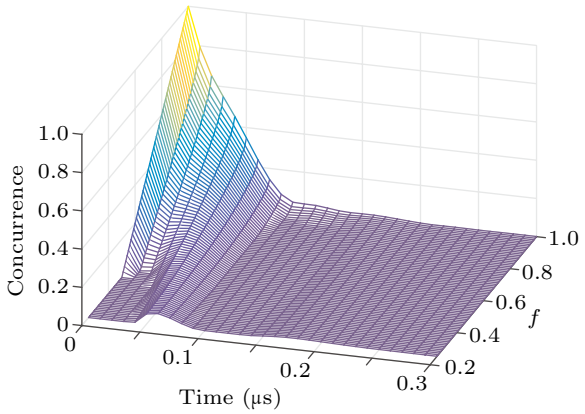


Fig. 6. Time evolution of the concurrence for initial Werner state $\rho_{\rm W}$ at $\lambda/x_2 = 1.2$.

3.4. Finite exchange coupling, finite collective relaxation

By tuning the qubits' frequencies slightly far away from $\lambda = 1.2x_2$, to e.g., $\lambda = 1.3x_2$, a regime, in which both the exchange coupling and the collective relaxation are non-zero $g_x \approx -2\pi \times 3.08$ MHz and $\Gamma_{\rm col} \approx -2\pi \times 4.25$ MHz, is reached.

The time evolution of the concurrence, as shown in Fig. 7, is similar to that shown in Fig. 5, even though the individual relaxation rates $\Gamma_a \approx 2\pi \times 5.63$ MHz and $\Gamma_b \approx 2\pi \times 3.26$ MHz are quite different from those in Subsection 3.2.

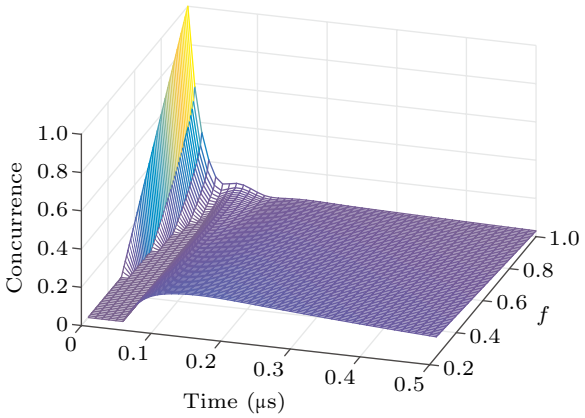


Fig. 7. Time evolution of the concurrence for initial Werner state $\rho_{\rm W}$ at $\lambda/x_2 = 1.3$.

To be clear, we have tacitly accepted that the frequency shifts of qubits does not contribute to entanglement. For example, at two special points $\lambda/x_2 = 1.5$ and $\lambda/x_2 = 3.0$, all variables are the same except for the frequency shift of qubit-a, as shown in Figs. 2 and 3. Comparing Fig. 8 with Fig. 5, the entanglement evolution is exactly the same at these two points, i.e., the concurrence is independent of the frequency shift of qubits. Subsequently, we also summarize the time $t_{\rm ESD}$ and $t_{\rm Rev}$ of ESD and revivals, respectively, for the above four cases in Table 1 (considering $f = 0.6$). By comparing the four cases, we may make a summary for entanglement revival, a common reservoir is more important than a qubit–qubit exchange coupling.

Table 1. The individual relaxation rates Γ_a, Γ_b, the collective relaxation rate $\Gamma_{\rm col}$, the exchange coupling strength g_x, and the entanglement sudden death time ($t_{\rm ESD}$) as well as the revival time ($t_{\rm Rev}$) versus the wavelength λ/x_2 ($f = 0.6$ is considered).

λ/x_2	Γ_a (MHz)	Γ_b (MHz)	$\Gamma_{\rm col}$ (MHz)	g_x (MHz)	$t_{\rm ESD}$ (μs)	$t_{\rm Rev}$ (μs)
2.0	$2\pi \times 0.03$	$2\pi \times 0.03$	0	0	2.31	
1.5	$2\pi \times 2.53$	$2\pi \times 10.03$	$-2\pi \times 5$	0	0.01	0.04
1.2	$2\pi \times 7.53$	$2\pi \times 0.03$	0	$-2\pi \times 4.33$	0.08	0.15
1.3	$2\pi \times 5.63$	$2\pi \times 3.26$	$-2\pi \times 4.25$	$-2\pi \times 3.08$	0.01	0.05

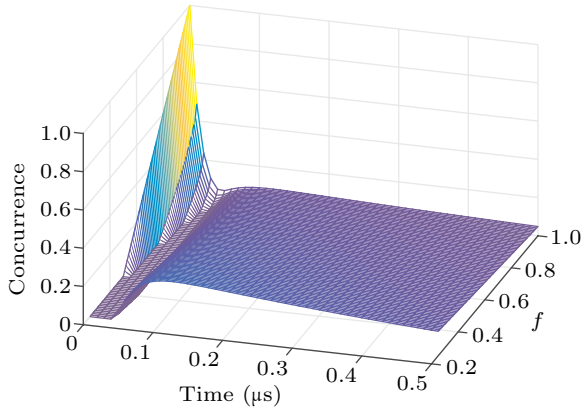


Fig. 8. Time evolution of the concurrence for initial Werner state $\rho_{\rm W}$ with $\lambda/x_2 = 3.0$.

4. Procedure for observing ESD and revival in waveguide QED

Though the Werner state has been frequently used for studying bipartite entanglement, experimentally generating such a state, especially with superconducting qubits, is hard. So far the Werner state has been successfully prepared in optical system.[31] Therefore, here we introduce a new type of X shape state similar to the Werner state

$$\rho_{\rm PW} = \frac{1}{4}\begin{pmatrix} f/2 & 0 & 0 & 0 \\ 0 & 1+f & {\rm i}\sqrt{3}f & 0 \\ 0 & -{\rm i}\sqrt{3}f & 3f/2 & 0 \\ 0 & 0 & 0 & 3(1-f) \end{pmatrix}, \tag{4}$$

and we call it pseudo-Werner (PW) state.

4.1. Preparing pseudo-Werner state

The PW state can be easily generated in our waveguide QED model system, with an auxiliary qubit (qubit-c in Fig. 1). We assume that the coupling between qubit-a and qubit-b (with the strength g), as well as the coupling between qubit-b and qubit-c (with the strength g_{bc}), have exchange form

$$\boldsymbol{XY} = \sigma_- \otimes \sigma_+ + \sigma_+ \otimes \sigma_-, \tag{5}$$

and that these couplings are switchable. The procedure for generating the PW state is as follows.

Initially, the three qubits are in a product state

$$\rho_1 = \rho_c \otimes \rho_b \otimes \rho_a, \tag{6}$$

in which qubit-a is prepared in a mixed state

$$\rho_a = \begin{pmatrix} f & 0 \\ 0 & 1-f \end{pmatrix}, \tag{7}$$

qubit-b and qubit-c are prepared in their excite state and ground state, respectively

$$\rho_b = \begin{pmatrix} 0 & 0 \\ 0 & 1 \end{pmatrix}, \ \rho_c = \begin{pmatrix} 1 & 0 \\ 0 & 0 \end{pmatrix}. \tag{8}$$

A method to prepare qubit-a to the mixed state ρ_a is described in Appendix B in details.

Secondly, by switching off the coupling between qubit-b and qubit-c, $g_{bc} = 0$, as well as tuning qubit-a's and qubit-b's frequencies to let $\lambda/x_2 = 2$, i.e., $g_x = \Gamma_a = \Gamma_b = \Gamma_{\rm col} = 0$ (see Figs. 2 and 3), only the exchange coupling g between qubit-a and qubit-b is non-zero. Using this non-zero exchange coupling to generate the evolution

$$\rho_2 = \mathrm{e}^{\frac{\mathrm{i}\pi}{4} I\otimes XY} \rho_1 \mathrm{e}^{\frac{-\mathrm{i}\pi}{4} I\otimes XY}, \tag{9}$$

we get the state

$$\rho_2 = \begin{pmatrix} 0 & 0 & 0 & 0 & 0 & 0 & 0 & 0 \\ 0 & f/2 & \mathrm{i}f/2 & 0 & 0 & 0 & 0 & 0 \\ 0 & -\mathrm{i}f/2 & f/2 & 0 & 0 & 0 & 0 & 0 \\ 0 & 0 & 0 & 1-f & 0 & 0 & 0 & 0 \\ 0 & 0 & 0 & 0 & 0 & 0 & 0 & 0 \\ 0 & 0 & 0 & 0 & 0 & 0 & 0 & 0 \\ 0 & 0 & 0 & 0 & 0 & 0 & 0 & 0 \\ 0 & 0 & 0 & 0 & 0 & 0 & 0 & 0 \end{pmatrix}, \tag{10}$$

where I denotes the single-qubit identity operator.

Then, we switch off the coupling g between qubit-a and qubit-b, and turn on the coupling g_{bc} between qubit-b and qubit-c. The non-zero exchange coupling can generate evolution

$$\rho_3 = \mathrm{e}^{\frac{\mathrm{i}\pi}{6} XY\otimes I} \rho_2 \mathrm{e}^{\frac{-\mathrm{i}\pi}{6} XY\otimes I}, \tag{11}$$

and produce a three-qubit state

$$\rho_3 = \begin{pmatrix} 0 & 0 & 0 & 0 & 0 & 0 & 0 & 0 \\ 0 & f/2 & \mathrm{i}(1/4)\sqrt{3}f & 0 & f/4 & 0 & 0 & 0 \\ 0 & -\mathrm{i}(1/4)\sqrt{3}f & 3f/8 & 0 & -\mathrm{i}(1/8)\sqrt{3}f & 0 & 0 & 0 \\ 0 & 0 & 0 & -(3/4)(-1+f) & 0 & \mathrm{i}(1/4)\sqrt{3}(-1+f) & 0 & 0 \\ 0 & f/4 & \mathrm{i}(1/8)\sqrt{3}f & 0 & f/8 & 0 & 0 & 0 \\ 0 & 0 & 0 & -\mathrm{i}(1/4)\sqrt{3}(-1+f) & 0 & (1-f)/4 & 0 & 0 \\ 0 & 0 & 0 & 0 & 0 & 0 & 0 & 0 \\ 0 & 0 & 0 & 0 & 0 & 0 & 0 & 0 \end{pmatrix}. \tag{12}$$

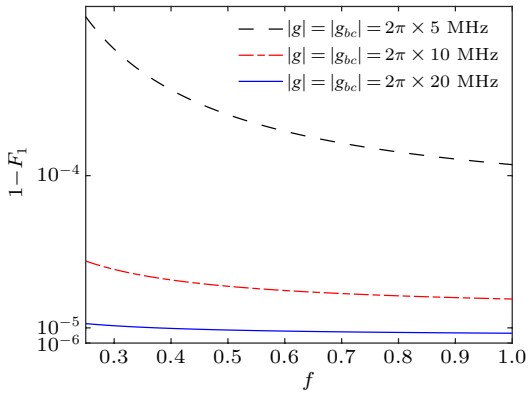


Fig. 9. The state infidelities $1-F_1$ of pseudo-Werner state versus the purity parameter f for different coupling strengths. $|g| = |g_{bc}| = 2\pi \times 5$ MHz, $2\pi \times 10$ MHz, and $2\pi \times 20$ MHz correspond to the black, red, and blue lines, respectively.

By partially tracing out the auxiliary qubit-c from ρ_3, the subsystem of qubit-a and qubit-b is finally in the PW state as Eq. (4). The state infidelity caused by the qubits' non-radiative decays can be minimized by choosing large enough coupling strengths g and g_{bc}, since the larger coupling strengths the shorter state preparation time. The PW state fidelity can be defined as[1]

$$F_1 = \mathrm{tr}\left(\sqrt{\sqrt{\rho_{\rm act}}\rho_{\rm PW}\sqrt{\rho_{\rm act}}}\right), \tag{13}$$

where $\rho_{\rm act}$ is the actual state generated by the procedures described above. We calculate the infidelity $1-F_1$ of the generated state by taking $g = g_{bc}$. As shown in Fig. 9, for coupling strengths $|g| = |g_{bc}| > 2\pi \times 10$ MHz, the non-radiative decays induced state infidelity can be smaller than 0.01%.

4.2. Time evolution of entanglement for initial pseudo-Werner state

Before studying the dynamics of the entanglement for pseudo-Werner state, let us consider the concurrence of $\rho_{\rm PW}$ itself. For $\rho_{\rm PW}$, the concurrence is simply (see Appendix A)

$$C = 2\max[0, F, G], \tag{14}$$

where

$$F = \sqrt{3}[2f - \sqrt{2f(1-f)}]/8, \ \ G = -\sqrt{3f(1+f)/32}. \tag{15}$$

Since $0.25 \le f \le 1$, obviously $G < 0$ for all values of f. Thus the concurrence is determined by F. The solution of the equation $F = 0$ is $f = 1/3$, which means that for $f \le 1/3$ the pseudo-Werner state is separable. The maximum concurrence $C = \sqrt{3}/2 \approx 0.866$ is reached at $f = 1$.

We then calculate time evolutions of the concurrences for the PW initial state with the same parameters and wavelengths

as those in Section 3. The concurrences are plotted in Fig. 10. Comparing the concurrences in Fig. 10 with those in Figs. 4–7, we can find that the entanglement dynamics of the PW state behaves very similar to that of the Werner state. Nevertheless, the concurrence of PW state has a obvious differences from Werner state for the case $\lambda/x_2 = 1.2$, i.e., finite exchange coupling, no collective relaxation. As shown in Fig. 10(c), the max entanglement of PW state caused by exchange coupling all exceed 0.2 across all the values of f comparing to the case of Werner state in Fig. 6. Moreover, comparing to Werner state, the first time of entanglement revival of PW state is shorter. Due to the simplicity of preparing the PW state, $\rho_{\rm PW}$ can become an ideal experimental toy for investigating bipartite entanglement.

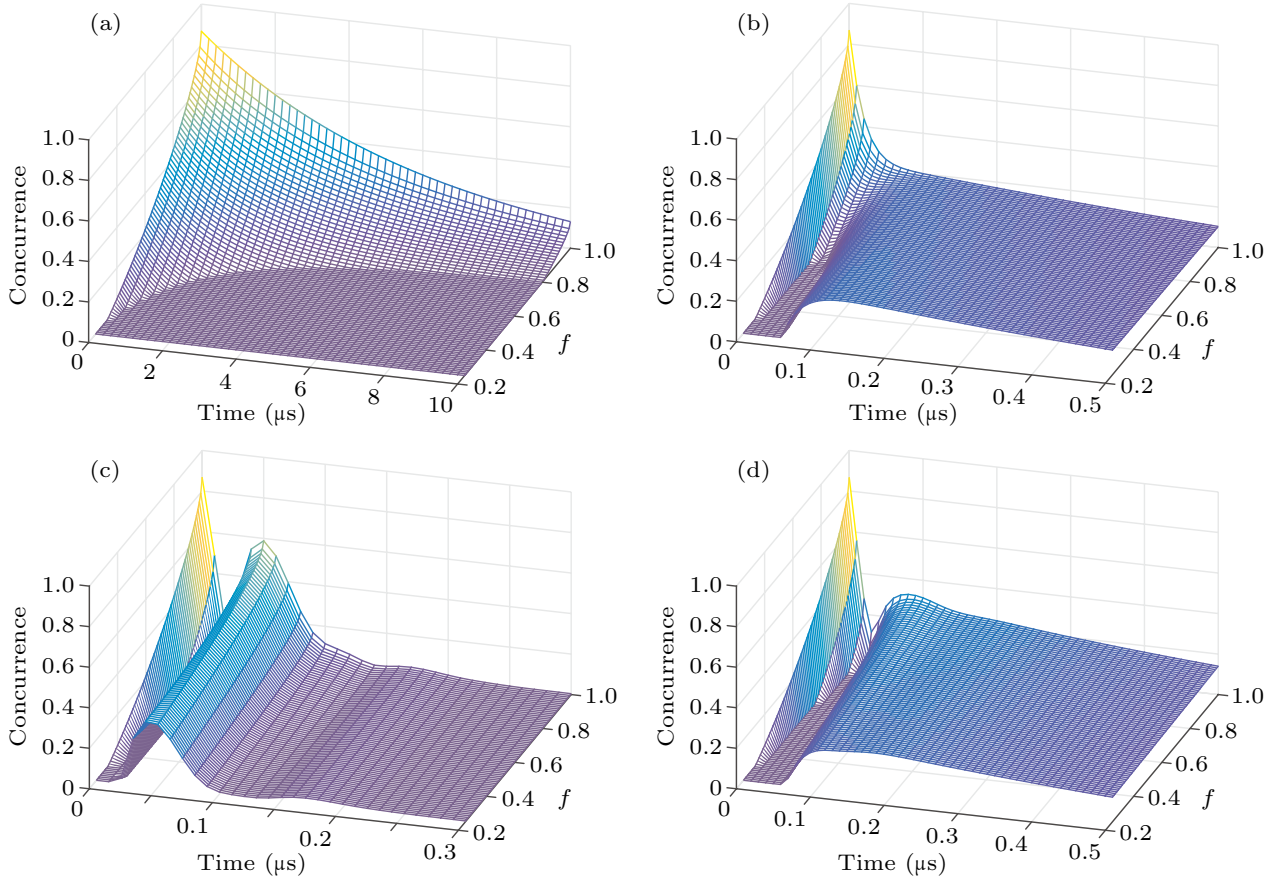


Fig. 10. Time evolution of the concurrence for initial pseudo-Werner state $\rho_{\rm PW}$ at (a) $\lambda/x_2 = 2$, (b) $\lambda/x_2 = 1.5$, (c) $\lambda/x_2 = 1.2$, and (d) $\lambda/x_2 = 1.3$.

4.3. Design of waveguide QED

Superconducting qubits' transition frequencies are in GHz range. Due to the limitation of bandwidth of the high performance cryogenic rf components such as low noise cryogenic amplifiers and circulators, superconducting qubit readout resonator for dispersive measurements is normally designed between 4 GHz and 8 GHz. In this waveguide QED system, let us assume that the readout resonators for qubit-a and qubit-b are at about 8 GHz. Then in order to be able to perform dispersive readout of the qubits, the maximum transition frequency should not higher than 7 GHz for both qubits.

The qubit frequency dependent wavelength

$$\lambda = 2\pi v_{\rm ph}/\omega_a, \tag{16}$$

where $v_{\rm ph}$ is the phase velocity in the waveguide. We use a conventional CPW design for the waveguide. Considering that the substrate is sapphire ($\varepsilon_{\rm r} = 9.8$), and that the metal parts of the CPW are fabricated by aluminum (since the kinetic inductance of aluminum is small), the characteristic impedance Z_0 and the phase velocity $v_{\rm ph}$ are calculated by Ref. [32].

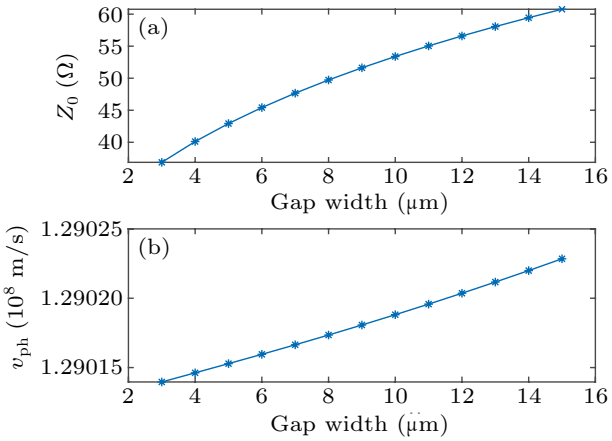


Fig. 11. (a) Characteristic impedance Z_0 versus vacuum gap width. (b) Phase velocity $v_{\rm ph}$ versus vacuum gap width.

By fixing the centre conductor width to 20 μm, as shown in Fig. 11, when the vacuum gap width is 8 μm, the characteristic impedance of the waveguide matches to 50 Ω, and the phase velocity $v_{\rm ph} \approx 1.29017 \times 10^8$ m/s. As mentioned above the maximum qubit frequency $\omega_a = 2\pi \times 7$ GHz, corresponding to a wavelength $\lambda \approx 18.4$ mm. Thus we can design the distances $x_1 = 9.2$ mm and $x_2 = 18.4$ mm, so that $\lambda/x_2 = 1$ (see Figs. 2 and 3) can be reached. For $\lambda/x_2 = 3$, the qubit frequency needs to be tuned to $\omega_a \approx 2\pi \times 2.3$ GHz, which might be too low for a dual-junction transmon qubit, however, $\lambda/x_2 = 2.4$ should be feasible at qubit frequency $\omega_a \approx 2\pi \times 3$ GHz.

5. Conclusion

We have shown the phenomena of ESD and entanglement revival for different X shape initial states under individual and collective decays utilizing a superconducting waveguide QED system. We find for both the Werner state and the pseudo-Werner state, the evolution of concurrence is dependent heavily on the wavelength determined by qubits' transition frequencies. We later demonstrate a detailed experimental procedure to observe ESD and revival in the superconducting waveguide QED system. The results may contribute to further understanding of the evolution of entanglement in dissipative quantum systems.

Appendix A: Concurrence calculation for X shape states

At any time t, the bipartite density matrix has the form

$$\rho(t) = \begin{pmatrix} a(t) & 0 & 0 & w(t) \\ 0 & b(t) & z(t) & 0 \\ 0 & z(t)^* & c(t) & 0 \\ w(t)^* & 0 & 0 & d(t) \end{pmatrix}. \tag{A1}$$

Substituting Eq. (A1) into Eq. (1), we can obtain the following kinetic equations of the non-zero density matrix elements:

$$\begin{aligned}
\dot{w}(t) &= -\frac{1}{2}w(t)[2(\gamma+\gamma_{\rm nr}) + 2{\rm i}(\omega_a+\omega_b) \\
&\quad +\gamma(\cos\phi+\cos 3\phi) + {\rm i}\gamma(\sin\phi+\sin 3\phi)], \\
\dot{z}(t) &= \frac{1}{2}\{-2z(t)(\gamma+\gamma_{\rm nr}) - 2{\rm i}z(t)(\omega_a-\omega_b) \\
&\quad +[2d(t)-b(t)-z(t)-c(t)]\gamma\cos\phi \\
&\quad +[2d(t)-b(t)-c(t)]\gamma\cos 2\phi - z(t)\gamma\cos 3\phi \\
&\quad +{\rm i}[b(t)-c(t)-z(t)]\gamma\sin\phi \\
&\quad +{\rm i}[b(t)-c(t)]\gamma\sin 2\phi + {\rm i}z(t)\gamma\sin 3\phi\}, \\
\dot{a}(t) &= [b(t)+c(t)](\gamma+\gamma_{\rm nr}) + [c(t)+z(t)+z(t)^*]\gamma\cos\phi \\
&\quad +[z(t)+z(t)^*]\gamma\cos 2\phi + b(t)\gamma\cos 3\phi, \\
\dot{b}(t) &= (\gamma+\gamma_{\rm nr})[d(t)-b(t)] \\
&\quad +\{d(t)-\frac{1}{2}[z(t)+z(t)^*]\}\gamma\cos\phi \\
&\quad -\frac{1}{2}[z(t)+z(t)^*]\gamma\cos 2\phi - b(t)\gamma\cos 3\phi \\
&\quad +\frac{1}{2}{\rm i}\gamma[z(t)-z(t)^*](\sin\phi+\sin 2\phi), \\
\dot{c}(t) &= (\gamma+\gamma_{\rm nr})[d(t)-c(t)] \\
&\quad -\{c(t)+\frac{1}{2}[z(t)+z(t)^*]\}\gamma\cos\phi \\
&\quad -\frac{1}{2}[z(t)+z(t)^*]\gamma\cos 2\phi + d(t)\gamma\cos 3\phi \\
&\quad -\frac{1}{2}{\rm i}\gamma[z(t)-z(t)^*](\sin\phi+\sin 2\phi), \\
\dot{d}(t) &= -d(t)[2(\gamma+\gamma_{\rm nr}) + \gamma(\cos\phi+\cos 3\phi)].
\end{aligned}$$

The concurrence is given by

$$C(\rho) = 2\max[0, F, G], \tag{A2}$$

where

$$F = |z| - \sqrt{ad}, \quad G = |w| - \sqrt{bc}.$$

Appendix B: Generating mixed state

Since normally a superconducting qubit has an intrinsic non-radiative decay with rate $\gamma_{\rm nr}$, this intrinsic decay can be utilized to generate the mixed state

$$\rho_a = \begin{pmatrix} f & 0 \\ 0 & 1-f \end{pmatrix} \tag{B1}$$

of qubit-a. Assuming initially the qubit is on its ground state, an on-resonance (with the qubit's transition frequency) Rabi pulse much longer than $1/\gamma_{\rm nr}$ drives the qubit into a mixed state

$$\rho_m \approx \begin{pmatrix} 1/2 & 0 \\ 0 & 1/2 \end{pmatrix}. \tag{B2}$$

We numerically calculate the time evolution of the density matrix diagonal elements $\rho_{\rm gg}$ (the ground state population), $\rho_{\rm ee}$ (the excited state population), and the absolute value of the off-diagonal element $\rho_{\rm eg}$, by taking $\gamma_{\rm nr} = 2\pi \times 0.03$ MHz and Rabi frequency $\Omega = 2\pi \times 30$ MHz. As shown in Fig. B1, a 35 μs long Rabi pulse can drive the qubit to the mixed state Eq. (B2).

After switching off the Rabi pulse, the off-diagonal density matrix elements remain zero, while the diagonal element $\rho_{\rm ee}$ ($\rho_{\rm gg}$) decays (increases) exponentially. Thus, depending on how long time to wait after the Rabi pulse, arbitrary fidelity factor $f \geq 0.5$ can be obtained. For example, $f = 0.8$ is reached 5 μs after the Rabi pulse, as shown in Fig. B1. Fidelity factor $f < 0.5$ can be realized by simply applying an extra π-pulse to flip the population.

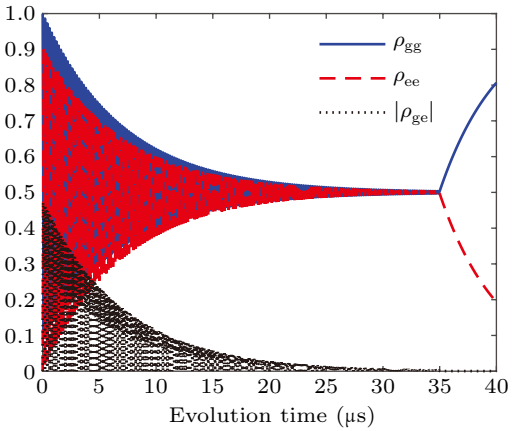


Fig. B1. Time evolution of the density matrix elements. The on-resonance Rabi pulse has a simple square envelope, which is switched on at $t = 0$ and switched off at $t = 35$ μs.

Acknowledgments

Project supported by the Key-Area Research and Development Program of Guangdong Province of China (Grant No. 2018B030326001), the National Natural Science Foundation of China (Grant No. 11874065), the Guangdong Provincial Key Laboratory (Grant No. 2019B121203002), the Science, Technology and Innovation Commission of Shenzhen Municipality (Grant No. KYTDPT20181011104202253), and the Shenzhen Hong Kong Cooperation Zone for Technology and Innovation of China (Grant No. HZQB-KCZYB-2020050).

References

[1] Nielsen M A and Chuang I 2000 *Quantum computation and quantum information* (Cambridge: Cambridge University Press) pp. 11–12
[2] Ekert A K 1991 *Phys. Rev. Lett.* **67** 661
[3] Grosshans F, Van Assche G, Wenger J, Brouri R, Cerf N J and Grangier P 2003 *Nature* **421** 238
[4] Bennett C H, Brassard G, Crépeau C, Jozsa R, Peres A and Wootters W K 1993 *Phys. Rev. Lett.* **70** 1895
[5] Bouwmeester D, Pan J W, Mattle K, Eibl M, Weinfurter H and Zeilinger A 1997 *Nature* **390** 575
[6] Bennett C H and Wiesner S J 1992 *Phys. Rev. Lett.* **69** 2881
[7] Mattle K, Weinfurter H, Kwiat P G and Zeilinger A 1996 *Phys. Rev. Lett.* **76** 4656
[8] Bennett C H, DiVincenzo D P, Shor P W, Smolin J A, Terhal B M and Wootters W K 2001 *Phys. Rev. Lett.* **87** 077902
[9] Peng X, Zhu X, Fang X, Feng M, Liu M and Gao K 2003 *Phys. Lett. A* **306** 271
[10] DiVincenzo D P 2000 *Fortschr. Phys.* **48** 771
[11] Yu T and Eberly J H 2004 *Phys. Rev. Lett.* **93** 140404
[12] Laurat J, Choi K S, Deng H, Chou C W and Kimble H J 2007 *Phys. Rev. Lett.* **98** 180504
[13] Almeida M P, de Melo F, Hor-Meyll M, Salles A, Walborn S P, Ribeiro P H S and Davidovich L 2007 *Science* **316** 579
[14] Ficek Z and Tanaś R 2006 *Phys. Rev. A* **74** 024304
[15] Xu J, Li C, Gong M, Zou X, Shi C, Chen G and Guo G 2010 *Phys. Rev. Lett.* **104** 100502
[16] Li J and Paraoanu G S 2009 *New J. Phys.* **11** 113020
[17] López C E, Romero G, Lastra F, Solano E and Retamal J C 2008 *Phys. Rev. Lett.* **101** 080503
[18] Das S and Agarwal G S 2009 *J. Phys. B: At. Mol. Opt. Phys.* **42** 205502
[19] Man Z X, An N B and Xia Y 2013 *J. Opt. Soc. Am. B* **30** 1092
[20] Shan C, Chen T, Liu J, Cheng W, Liu T, Huang Y and Li H 2010 *Chin. Phys. B* **19** 060303
[21] Al-Qasimi A and James D F V 2008 *Phys. Rev. A* **77** 012117
[22] Kockum A F, Johansson G and Nori F 2018 *Phys. Rev. Lett.* **120** 140404
[23] Kannan B, Ruckriegel M J, Campbell D L, Kockum A F, Braumüller J, Kim D K, Kjaergaard M, Krantz P, Melville A, Niedzielski B M, Vepsäläinen A, Winik R, Yoder J L, Nori F, Orlando T P, Gustavsson S and Oliver W D 2020 *Nature* **583** 775
[24] Wen P Y, Ivakhnenko O V, Nakonechnyi M A, Suri B, Lin J J, Lin W J, Chen J C, Shevchenko S N, Nori F and Hoi I C 2020 *Phys. Rev. B* **102** 075448
[25] Wen P Y, Lin K T, Kockum A F, Suri B, Ian H, Chen J C, Mao S Y, Chiu C C, Delsing P, Nori F, Lin G D and Hoi I C 2019 *Phys. Rev. Lett.* **123** 233602
[26] Yang C, Su Q, Zheng S and Han S 2013 *Phys. Rev. A* **87** 022320
[27] Yan F, Krantz P, Sung Y, Kjaergaard M, Campbell D L, Orlando T P, Gustavsson S and Oliver W D 2018 *Phys. Rev. Appl.* **10** 054062
[28] Wootters W K 1998 *Phys. Rev. Lett.* **80** 2245
[29] Bennett C H, Brassard G, Popescu S, Schumacher B, Smolin J A and Wootters W K 1996 *Phys. Rev. Lett.* **76** 722
[30] Li J and Paraoanu G S 2010 *Eur. Phys. J. D* **56** 255
[31] Barbieri M, De M F, Di N G and Mataloni P 2004 *Phys. Rev. Lett.* **92** 177901
[32] Simons R N 2001 *Coplanar Waveguide Circuits, Components, and Systems* (New York: John Wiley & Sons) pp. 12–16